EAI Endorsed Transactions
on Industrial Networks and Intelligent Systems Research Article EAI.EU

Application of Computer Vision in T-Shirt Dimensions Measurement

Ngoc-Bich Le[1,2*], Thi-Thu-Hien Pham[1,2], Quoc-Hung Phan[3], Narayan C. Debnath[4], Ngoc-Huan Le[4*]

[1]School of Biomedical Engineering, International University, Ho Chi Minh City, Vietnam
[2]Vietnam National University Ho Chi Minh City, Thu Duc City, Ho Chi Minh City, Vietnam
[3]National United University, Department of Mechanical Engineering, Miaoli, Taiwan
[4]Eastern International University, Binh Duong, Vietnam

Abstract

This paper presents a solution to automatically measure the T-shirt dimensions in the garment industry. To address this goal, the paper focuses on utilizing image processing to determine the T-shirt's dimensions. The processing algorithm was provided along with the proposed recognition regions novel approach that was expected to deliver faster processing speed and enhance accuracy. The feasibility was demonstrated by characterizing the accuracy and processing speed. Specifically, five distinctive dimensions were successfully identified and measured; with the replication of 30, the discrepancy varies from 0.095% (for chest) to 2.088% (for collar). The divergence is insignificant compared with the granted tolerances. Finally, the processing time and the mechanical structure of the system deliver productivity of 22 products/minute which is approximately 10 times more rapidly than manual measurement (25 seconds).

Keywords: T-Shirt, Auto-dimensioning, computer vision, metrology automation, intelligent system.

Received on 12 January 2022, accepted on 21 April 2022, published on 29 April 2022

doi: 10.4108/eetinis.v9i31.707

*Corresponding author. Email: lnbich@hcmiu.edu.vn, huan.le@eiu.edu.vn

1. Introduction

In recent years, automatic inspection by computer vision technology has been widely used in the production process to provide manufacturers the opportunity to enhance product quality and reduce costs. Computer vision systems can benefit the company's automated production stages by replacing workers in processes such as: checking product defects, monitoring surface quality, and checking product sizes with high precision.

In [1], John et al. focus on the development of the vision system for the measurement and inspection of bolts. In this work, the authors mainly build on the self-learning convolutional neural network to use computer vision technology for detecting defects. Similarly, instead of using workers to visually check product quality, the authors in [2],[3] proposed solutions to inspect this process automatically. The results published are impressive with the improved performance and stability of the inspection system. The image processing technology is also used for error checking in the golf club manufacturing process as seen in the paper [4].

For factories manufacturing the printed circuit board assembly (PCBA), the inspection of the quality of weld joints, the number of components, the position and direction of components, ... are now based on the help of AOI machines using image processing technology. In [5-8] the authors reported new studies to be able to test most of the defects that might appear during actual production. To aid in the checking of dimensions, stereo vision-based measurement methods have been developed and applied in many fields, including distance measurement, deformation measurement, and object reconstruction of 3-dimensional objects [9-12]. Computer vision systems that combine multiple cameras or combine a camera with multiple sensors are also widely used in measuring the size of objects in industrial applications [13], [14].

In the footwear industry, a novel gluing machine comprising a Cartesian robot and a vision system was presented in [15]. The vision system supports locating and reconstructing the shape of objects to be glued. The identified information is then used to plan the trajectory of the robot carrying the glue gun and to move the robot.

In the garment industry, to the high-quality T-shirt manufacturing field of famous brands such as Nike, Adidas... the requirements for product quality, especially product dimensions, are very strict. In practical production, a product is produced with many different standard sizes to fix different customers. This raises the issue that every product needs a certain accuracy of the correlation between the dimensions. Especially, there is some required tolerance on significant dimensions of a T-shirt comprising chest width, bottom width, shoulder width, neck width, sleeve length, sleeve width, shirt length... These dimensions are related closely to ensure standard product size. However, the current dimension inspection is mostly performed by hand. This leads to consequences such as low productivity (about 25 seconds per one measurement), large error, high cost... Consequently, the demand for automated inspection with fast processing speed, high accuracy... was requested by industrial to improve productivity, increase product quality and reduce workspace. In [16], Karunamoorthy and Ramprabu presented a technique to measure the sizes of a garment from a single picture. POLO Company's t-shirt was used to measure standard parameter values. In this study, the authors measured only the height and width parameters of the t-shirt. And the accuracy of 98% from the value of POLO company's measurement was reported. In [17], a new visual perception architecture was proposed to analyse clothing configurations. This architecture is integrated with active stereo vision and a dual-arm CloPeMa robot to grip and flatten clothes. The system analysed the general 3D surface and tended to fully understand landmark structures distributed on the clothing surface. As a result, the system exhibits adaptability for multiple visually-guided clothes manipulation tasks.

The automatic inspection machine provides high processing speed as well as great support for workers. Regularly, the worker handles the inspected t-shirt firmly on the vacuum table then measures each dimension by hand. The measured results are then manually recorded and evaluated. With an automatic inspection machine, the worker is just involved in handling the shirt on the table, measuring will be conducted by the machine automatically. This helps avoid the objective natures of humans such as bad mood, fatigue, tiredness, confusion... Furthermore, the measured database can be processed, analysed, saved and retrieved easily.

Consequently, this research focused on developing a system for inspecting the t-shirt dimensions automatically to fulfill the expected productivity of 15 to 20 products/minute. The computer vision was applied to detect the T-shirt's standard dimensions. The measured results demonstrated stable results compared to those of a manual job. The feasibility of the proposed novel approach was validated by practice operation on the industrial shop floor.

2. Mechanical Design

The proposed structure was designed to meet the desired operational productivity of 15-20 shirts/minute, see Figure 1. When one shirt is in the process, including handling and processing, the workers at the remaining three stations have time to perform their handling operation. Specifically, the waiting time for a station is estimated to be (5 ~ 6) x3 = 15 ~ 18 seconds, this time is quite enough for a worker to ensure his task.

The structure consists of four measuring tables at four corners with the camera in the centre position. This option ensures work productivity, creates a comfortable time for workers while spreading the shirt, thereby minimizing distortion caused by wrinkles, improving the quality of image processing as well as the final result. The first structural cluster is the measuring table. The table slides on two sliders and is driven by an AC servo motor through a timing belt system. This structure ensures fast travel, precise speed and position control, and low noise. The second structural cluster is the image processing box. The camera is located in the middle of the box's ceiling. The LED matrix consisting of 50x50 dimmable LEDs is arranged on the ceiling of the image processing box to ensure the uniformity of light and the most suitable light intensity.

The operation of the system can be briefly described as follows: (1) When the operator at the first station finishes spreading the shirt, he presses the finish button, the first slide will be transported into the image processing box, taking pictures, and process the results. The shirt is then transferred back to its original location with a good (G) or not good (NG) product indicator light. An operator will process according to the displayed results. Sequentially, the operator at the 2nd station has now finished spreading the shirt and the same process goes on. Similarly and sequentially for stations 3, and 4. As can be seen, the time allowed for the operator to process 1 shirt is equal to the total transport and processing time of three stations. This ensures sufficient processing time at the stations and takes advantage of the continuous processing performance of the image processing box.

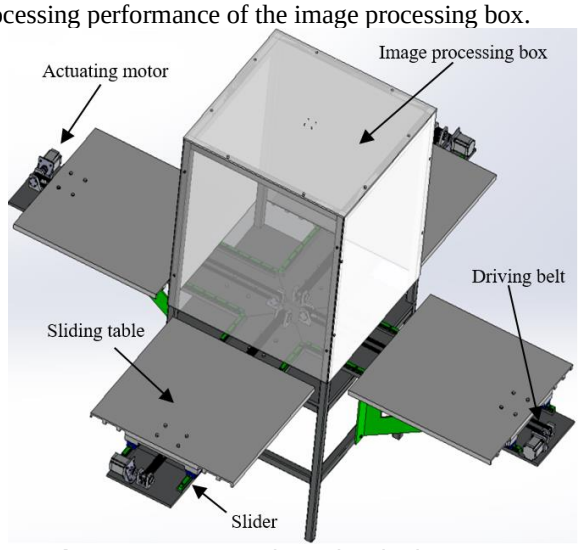

Figure 1. Proposed mechanical structure.

FEM analysis results of the proposed structure are shown in Figure 2. It is evident that the resulted stress and deformation are in the acceptable domain. Specifically, the maximum deformation is 6.737e-001 mm and maximum von Mises stress is 51.964 MPa compared to the permissible values of 1mm and 248.168 MPa (Yield strength), respectively. These results prove the applicability of the designed structure.

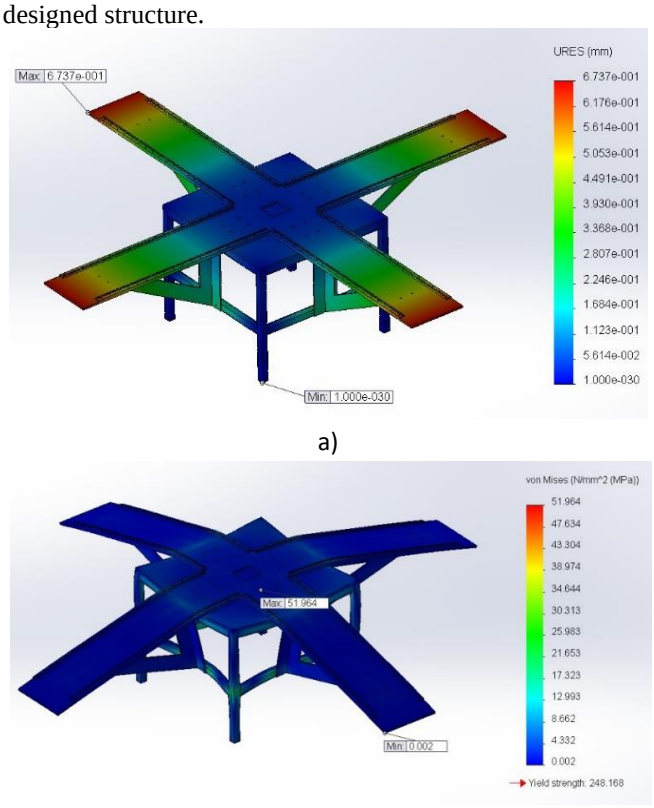

Figure 2. FEM analysis results: a) Deformation and b) von Mises stress.

3. Experimental Setup

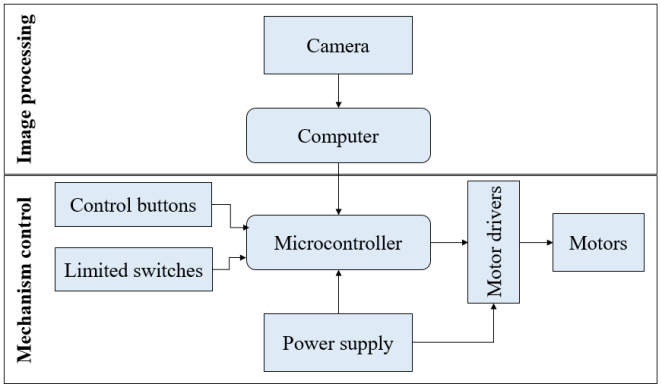

Figure 3. Experimental setup.

The experimental setup presented in Figure 3 is comprised of (1) one motor driven by a power driver to actuate the sliding vacuum table; (2) one processor unit to control the sliding table and to communicate with a computer via Max 232 unit; (3) control buttons to handle the table; (4) limit switches to limit sliding table operating path; (5) one computer to process data; and (6) one camera to capture the image. The utilized computer hardware configuration consists of Intel Core i5 2.5 GHz CPU and 8.0 GB Ram.

4. Image Processing

4.1 Homography matrix

In computer vision, projective homography is at the core of many complications in image registration. Planar homography is a projection from this plane to the other plane. In this study, measurements were carried out on the plane, therefore, planar homography was applied to transform the pixel coordinates into physical coordinates. H is defined as a Homography matrix. H matrix shows the relationship between points on a real plane and the corresponding pixel in the image obtained from the camera. The following equation represents this correlation [18].

$$p_{dst} = H.p_{src},\ p_{src} = H^{-1}.p_{dst} \quad (1)$$

Where: $p_{dst} = \begin{bmatrix} x_{dst} \\ y_{dst} \\ 1 \end{bmatrix}, p_{src} = \begin{bmatrix} x_{src} \\ y_{src} \\ 1 \end{bmatrix}$, (2)

x_{src}, y_{src} are source coordinate and x_{dst}, y_{dst} are destination coordinate,

p_{src} is source point/pixel and p_{dst} is destination point/pixel.

H matrix can be established without experiencing the internal parameters of the camera. Practically, the determination of the H matrix from snapshots of the same object can be used to regulate the internal parameters of the camera.

OpenCV library provides a function called cvFindHomography() which is utilized to determine the H matrix when the corresponding points on the two planes are perceived. Determination of H matrix requires at least 4 corresponding points (3 points do not line up) on two planes. The more corresponding points are applied the better the noise filterability. This study used the chessboard applied in the camera calibration to achieve this task.

4.2 Image processing

The image processing process demonstrated in Figure 4 comprises four main steps including grayscale, binary, boundary extract, and search for reference points. In this study, the fourth step is the critical step that influents the speed and quality of the processing results. Recognition regions were proposed and applied to deliver a faster processing speed and to reduce processing failures. The

detail of this issue will be discussed more in the subsequent section.

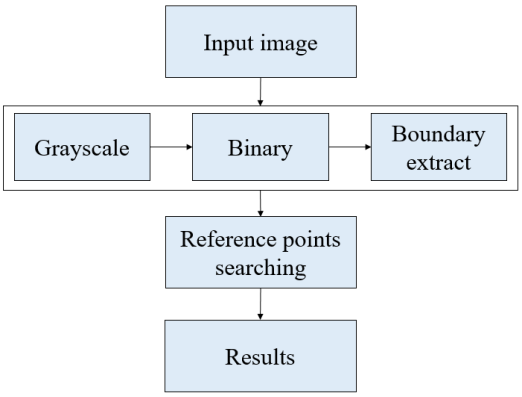

Figure 4. Image processing process.

4.2.1 Grayscale

According to the standard colour system NTSC (National Television System Committee), a grayscale image of a colour image can be appraised by each respective pixel using the following formula:

$$Y = YR + YG + YB = \alpha . R_d + \beta . G_d + \delta . B_d \quad (3)$$

Where:

Y is the gray level value of the pixel

R_d, G_d, B_d are values of the primary colour pixel R (red), G (green), B (blue).

α, β and δ are 0.299, 0.587 and 0.114, respectively.

Figure 5. Grayscale image.

The obtained grayscale image was then threshold partitioned to regulate the inside-outside areas, as shown in Figure 5. The threshold is an intimate concept in image processing algorithms. It refers to a value that the algorithm relies on to partition a set into distributed domains. The threshold value is usually established based on the special points (eg. the average), or based on the experience. If considering the number of thresholds applied to the same data set, there exist three kinds of threshold partitions including single-threshold, dual-threshold, and multi-threshold.

If based on the discrepancy of the threshold value, there are two methods including fixed threshold and adaptive threshold. An adaptive threshold means its value will change accordingly to the deviation of the data set in space and time. Regularly, this value is regulated using statistical methods. The obtained image by utilizing a partition threshold was presented in Figure 6.

Figure 6. Partition threshold result.

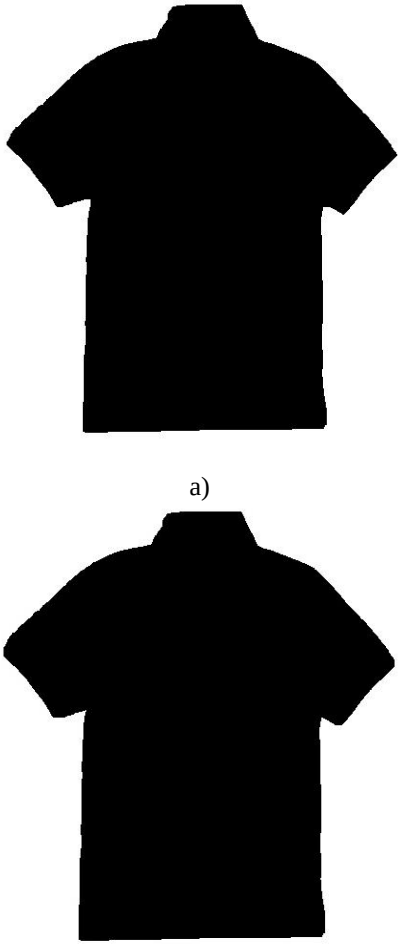

a)

b)

Figure 7. a) Eroded filter result, b) Dilate filter result.

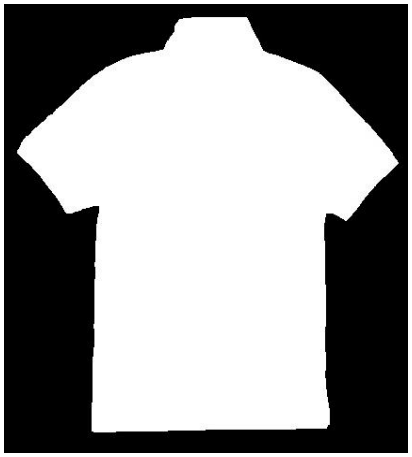

Figure 8. Invert filter result.

The acquired image incorporates the inside and outside areas of the shirt. It is evident that some noises still exist. These noises are the result of wrinkles, daisies, etc., and can be enhanced by applying some morphological operations for image enhancement such as Dilation, and Erosion operations.

By exploiting the erosion operation, small blobs were wiped out and favourable results were obtained as shown in Figure 7a. It is evident that noises caused by buttons and borders were removed. However, with this operation, the image deformed significantly; the dimensions became bigger than the original ones, and more rounded corners were produced. These drawbacks significantly affect the accuracy when the product dimensions are measured. Consequently, a dilation operation with the same structuring element was applied. After implementing the Dilation operation, the attained image delivered fewer jagged edges and was displayed in Figure 7b. The noise generated by buttons and borders was completely filtered out. There is no significant diversity in dimensions compared to the original image. Afterward, the inverting algorithm was deployed to convert the object's and the background colour to white and black, respectively. The result was exhibited in Figure 8.

4.2.2 Boundary extraction

The boundary profile model is mathematically represented based on pixel grayscale variation u(x) as shown in Figure 9.

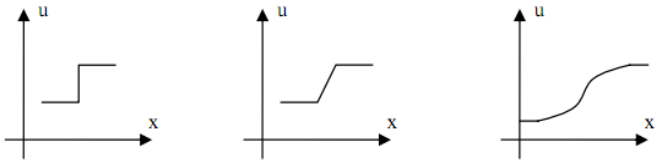

a) b) c)

Figure 9. Image boundary profiles: a) ideal profile, b) stepped profile, and c) real profile.

In this application, a direct border detection algorithm was deployed with the essential boundary separation comprising Sobel, Laplace, Canny operators. These functions are available in the OpenCV library.

Images acquired from three filter operators, Sobel, Laplace, and Canny were presented in Figure 10. It is obvious that the Canny filter delivers the most favourable result with less noise, thin edge, clarity, and continuity. Consequently, the Canny operator was nominated.

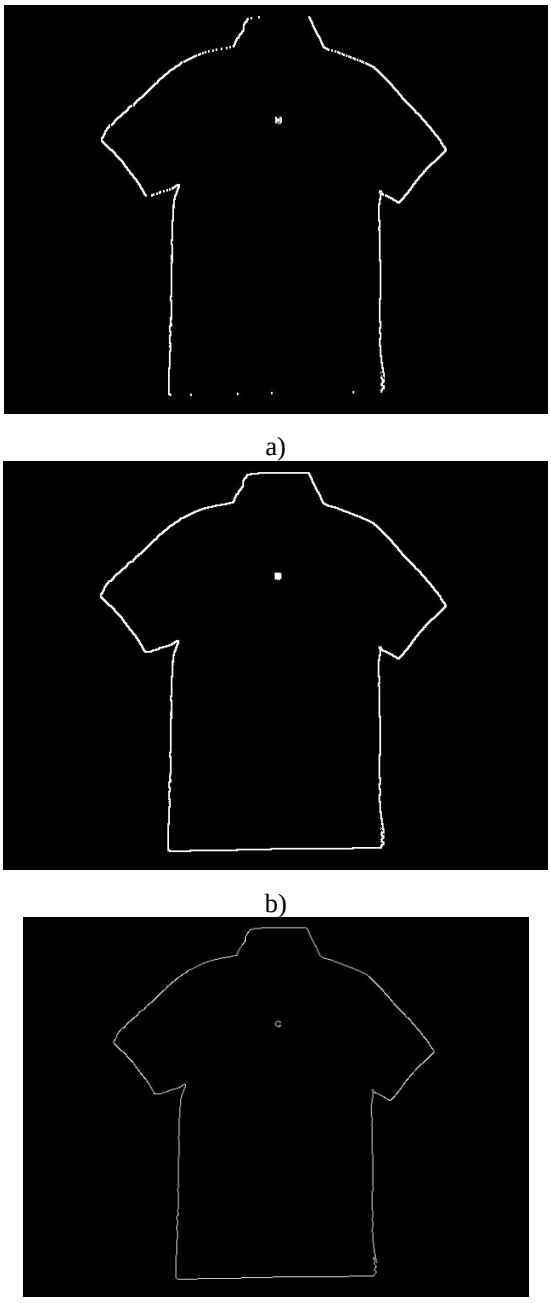

a)

b)

c)

Figure 10. Filter result: a) Sobel, b) Laplace, and c) Canny.

After conducting boundary extraction, the image was rotated so that the bottom line is horizontal to ensure processing accuracy. To achieve the rotation angle, the discrepancy between the bottom line and the horizontal line needs to be resolved as demonstrated in Figure 11.

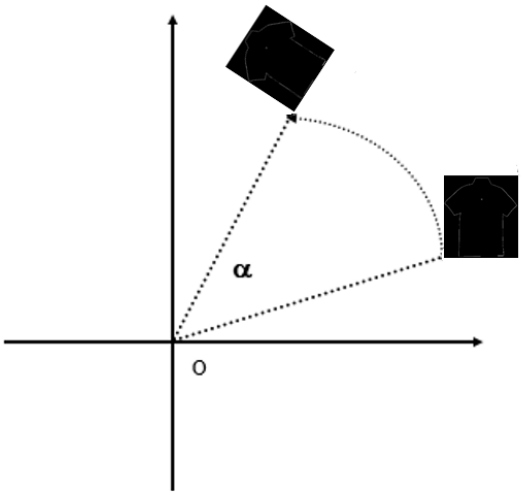

Figure 11. Definition of rotated centre and angle for Affine Transformation.

The Affine transformation was then applied to rotate the filtered image by utilizing the following matrix with a designated rotation angle and centre.

$$\begin{cases} x' = cos\alpha x - sin\alpha y \\ y' = sin\alpha x - cos\alpha y \end{cases} \leftrightarrow T(\alpha) = \begin{pmatrix} cos\alpha & -sin\alpha & 0 \\ sin\alpha & cos\alpha & 0 \\ 0 & 0 & 1 \end{pmatrix} \quad (4)$$

4.2.3 Dimension definition.

The determination of the dimensions of the shirt is based on the detection of predefined corner points, bending points, and neighbouring points. These points were delivered from the manual measuring process. These points were detected by scanning the extracted boundary image and finding the distinct characteristic of the target points from the remaining boundary points. In order to moderate the processing time and to avoid the interference of the points with the same characteristics, scanning was made within different image recognition regions (1 to 8). Every recognition region contains a corresponding target point. The predefined recognition regions were shown in Figure 12. The measurement of major dimensions is achieved as follows.

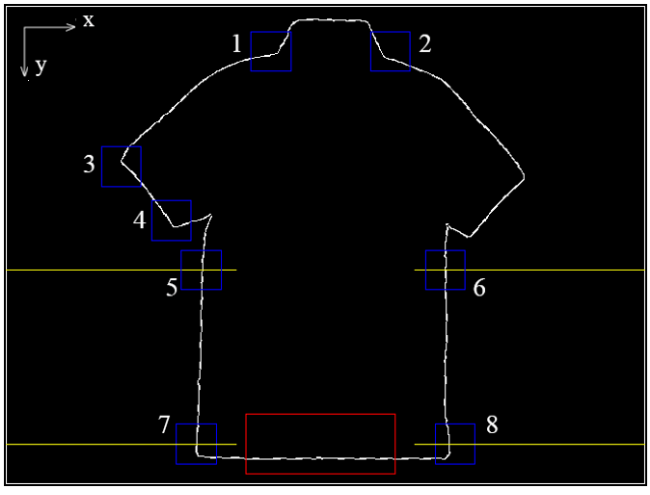

Figure 12. Defined recognition regions.

Chest width:

The chest width dimension is the length of line (a) in Figure 15 positioned about 5 to 7 centimeters under the armpits (based on the manufacturer's definition) and is formed by two boundary points scanned in regions 5 and 6. To levitate the accuracy, ten nearby lines in the defined area were detected and averaged.

Bottom width:

Identical to the determination of the chest width, the bottom width was attained by two characterized points in regions 7 and 8 as shown in Figure 15 (line b). The accuracy is also enhanced by taking the average value of a line set.

Sleeve width:

Sleeve width, line (c) in Figure 15, was attained by scanning the elbowed points found in Region 3 and Region 4. The red dots shown in Figure 13 are the elbowed points that need to be identified. These points were perceived based on their distinctive characteristics correlated to others. Specifically, it is obvious that the characterized points have the smallest X coordinate and largest Y coordinate in regions 3 and 4, respectively. The distance between these two points was anticipated by exploiting the Pythagorean theorem 2.

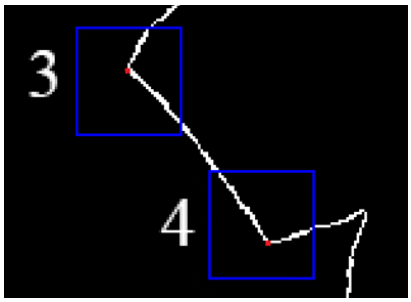

Figure 13. Characterized points of sleeve.

Collar width:

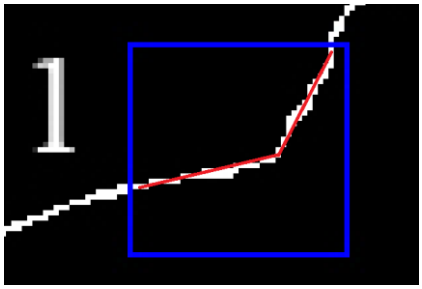

Figure 14. Bending characterized point of the collar.

Collar width, line (d) in Figure 15, is relatively more challenging to tackle than other items. To resolve this dimension, a bending point in Region 1 as shown in Figure 14 needs to be detected. This characterized point is the intersection of the collar and the shoulder boundary lines. In our algorithm, this inflection point was identified using 2 scanning loops for the 2 axis to search for the abrupt change in any axis coordinates. The same concept was applied to identify the characterized point in Region 2. The distance

between these two characterized points is the width of the collar. In order to boost the success of the identification process, a favourable quality image is required to avoid interference caused by wrinkles.

Shirt length:

Shirt length is the distance from the bending point in Region 1 defined previously to the bottom line. Shirt length was presented as line (e) in Figure 15. The processing algorithm was initiated from the bending point and the length is accumulated downward until meeting the boundary point on the bottom line.

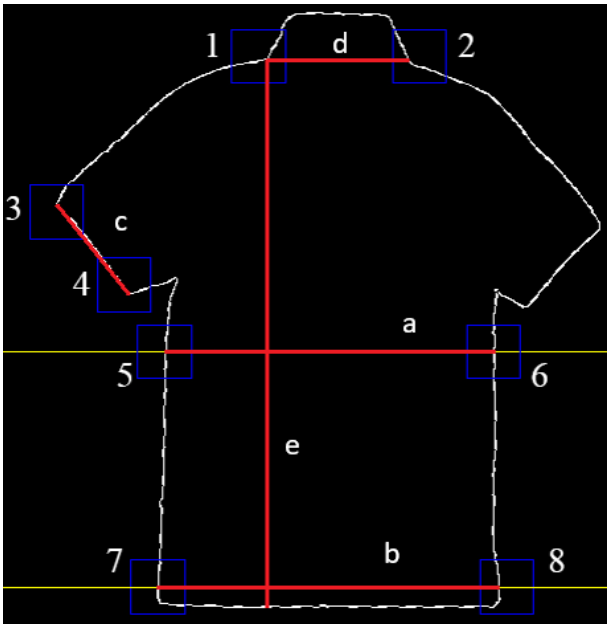

Figure 15. Predefined recognition regions and corresponding dimensions.

5. Experimental Results

Standard dimensions and corresponding allowable tolerance were presented in Table 1.

Table 1. Standard dimensions and allowable tolerance of M size t-shirt.

Items	Dimension (mm)	Tolerance (inch)	Tolerance (mm)	Tolerance (%)
1. Collar width	180	± 1/4	± 6,35	±3,528
2. Shoulder width	390	± 1/2	± 12,7	±3,256
3. Sleeve length	220	± 1/2	± 12,7	±5,773
4. Sleeve width	150	± 1/4	± 6,35	±4.233
5. Chest width	420	± 3/8	± 9,525	±2,268
6. Bottom width	430	± 3/8	± 9,525	±2,215
7. Length	700	± 3/4	± 19,05	±2,721

The experiment was conducted under the following experimental conditions:

- Light: 700 lx.
- Distance from camera to sliding table surface: 950mm.
- Sliding table background colour: White, reflectless.
- Image size: 640x480 pixels.
- T-shirt is carefully positioned on the sliding table surface.

The sample T-Shirt used in the experiment is a qualified product. Its manually measured dimensions are shown in Table 2. The sampling size is 30 replications.

Table 2. Sampled T-Shirt manually measured results.

Items	Mean	Standard Deviation
Bottom	436.1	2.83
Chest	419.5	2.34
Sleeve	152.5	1.45
Length	705.8	2.85
Collar	182.2	1.73

The experimental processing results were tabulated in Table 3. The time consumption for each measurement is shown in Table 4. After one experiment, the sample was re-handled to renew the measuring process.

Table 3. Experimental processing results (unit: mm).

Ex. Num.	1	2	3	4	5	6	7	8	9	10
Bottom	433.2	436.4	431.3	434.2	431.1	433.4	436.3	433.5	434.3	438.4
Chest	419.6	421.1	417.5	419.4	419.3	417.3	421.5	419.3	419.1	421.2
Sleeve	152.3	152.0	148.6	153.3	148.6	151.2	152.0	151.0	153.3	152.2
Length	704.7	704.7	703.0	703.0	703.0	703.0	704.7	704.7	703.0	704.7
Collar	175.3	180.2	178.7	177.8	180.2	178.1	180.2	177.7	177.7	180.6
Ex. Num.	**11**	**12**	**13**	**14**	**15**	**16**	**17**	**18**	**19**	**20**
Bottom	431.7	436.7	434.9	434.6	436.4	433.3	433.7	433.4	433.3	433.7
Chest	419.1	421.4	419.3	419.5	421.6	419.7	417.3	419.9	419.6	419.2
Sleeve	148.8	152.2	151.2	151.2	150.9	149.9	152.2	146.3	152.2	151.0
Length	706.4	704.7	703.0	704.7	704.7	703.0	703.0	704.7	704.7	704.7
Collar	178.3	180.3	178.5	177.2	180.7	178.4	178.8	178.3	177.7	177.8
Ex. Num.	**21**	**22**	**23**	**24**	**25**	**26**	**27**	**28**	**29**	**30**
Bottom	433.6	436.8	434.2	434.3	431.8	431.7	434.3	433.8	434.2	434.4
Chest	421.2	421.4	417.4	419.1	417.2	417.2	421.1	419.2	419.7	419.6
Sleeve	152.2	150.9	149.7	151.0	148.6	151.0	146.2	146.3	149.5	153.3
Length	704.7	704.7	704.7	703.0	703.0	703.0	704.7	704.7	704.7	703.0
Collar	180	180	178	178	178	178	178	178	177	177

Table 4. Processing time (unit: millisecond).

Ex. Num.	1	2	3	4	5	6	7	8	9	10
Pro. Time	528	590	578	625	570	578	612	534	589	546
Ex. Num.	**11**	**12**	**13**	**14**	**15**	**16**	**17**	**18**	**19**	**20**
Pro. Time	597	538	569	643	582	549	538	549	593	632
Ex. Num.	**21**	**22**	**23**	**24**	**25**	**26**	**27**	**28**	**29**	**30**
Pro. Time	638	582	547	611	596	574	532	594	616	597

Statistical analysis was conducted utilizing Origin Pro commercial package. With the replication of 30, the Means and Standard deviation of the bottom, chest, sleeve, length, and collar were obtained and presented in Table 5. A confidence of 95% was recorded.

Table 5. Experimental result statistical analysis.

Items	Mean	Standard Deviation
Bottom	433.6	1.73
Chest	419.1	1.38
Sleeve	150.6	2.01
Length	704.1	0.94

Collar	178.2	1.29

Figure 16 demonstrates the comparison of the processing results with manually measured and given standard values. It is obvious that the deviation is insignificant. The largest discrepancy of 3.8 mm (around 2%) was recorded. This discrepancy is relatively negligible compared to the allowable tolerance of the shirt granted in Table 1.

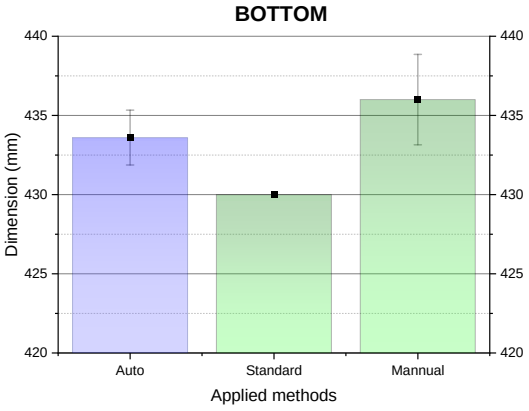

a)

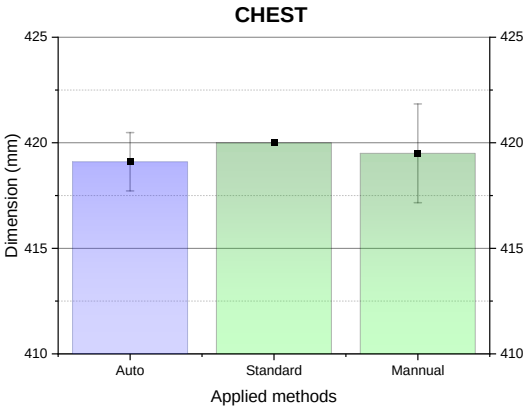

b)

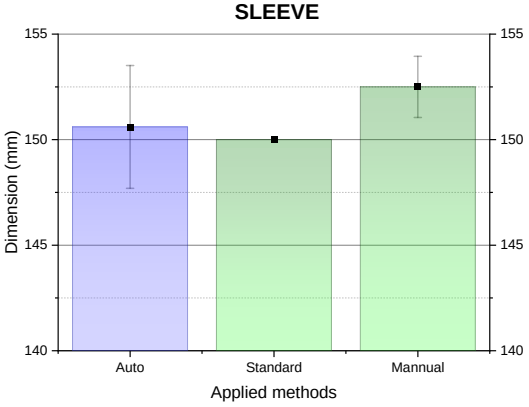

c)

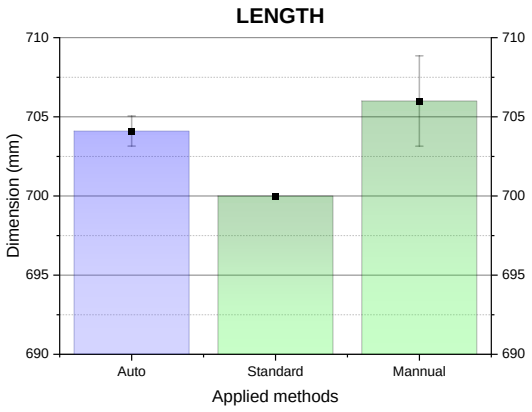

d)

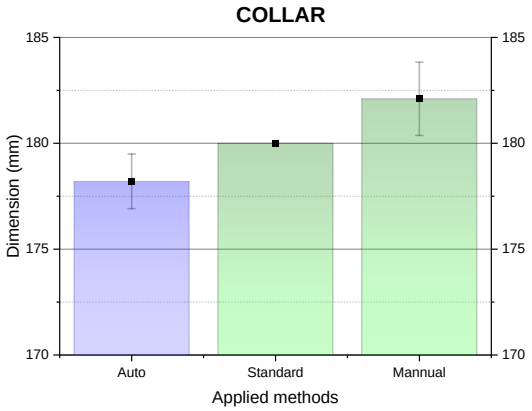

e)

Figure 16. Comparison of the proposed system and manually measured results of: a) Bottom, b) Chest, c) Sleeve, d) Length, and e) Collar dimension.

Finally, the processing time results in Table 4 were utilized to estimate the system's productivity. The longest time is 643 milliseconds recorded. The mechanical operation is approximately 2 seconds for each cycle. Consequently, the productivity of the system is approximately 22 products/minute.

6. Conclusion

In this study, a novel processing algorithm with pre-defined scanning regions approaches to produce faster processing speed and improve accuracy was proposed. With the suggested strategy, the complication of detecting the measuring T-shirt dimensions was solved successfully. The feasibility was demonstrated by determining the accuracy and processing speed. Specifically, five different dimensions were successfully identified and measured. With the replication of 30, the discrepancy compared to manual measurement varies from 0.095% (for chest) to 2.088% (for collar). This divergence is insignificant compared with the

granted tolerances. The processing time and the mechanical structure yield the productivity of 22 shirts/minute which is 10 times more rapid than manual measurement.

Acknowledgments.

We would like to express my very great appreciation to Esquel Garment Manufacturing (Vietnam) Co. Ltd for giving the demand and experimental material.

References

[1] John Rajan, A., Jayakrishna, K., Vignesh, T., Chandradass, J., Kannan, T.T.M., (2021) Development of computer vision for inspection of bolt using convolutional neural network, *Materials Today: Proceedings* **Volume** 46(7), pp. 6931-6935. DOI: 10.1016/j.matpr.2021.01.372

[2] Le, N. H., Tu, V. B. N., (2019) A Machine Vision Based Automatic Optical Inspection System for Detecting Defects of Rubber Keypads of Scanning Machine, *EAI Endorsed Transactions on Industrial Networks and Intelligent Systems*, **Volume** 6(18). DOI: 10.4108/eai.28-3-2019.157121

[3] Meng, Y. F., Gong, S. R., Liu, C. P., (2010) A Fast Computer Vision System for Defect Detection of Rubber Keypad, *2010 International Conference on Computer Application and System Modeling (ICCASM 2010)*, pp. V2-155-V2-160. DOI: 10.1109/ICCASM.2010.5620156

[4] Wu, S. H. P., Guo, H. Y., (2015) Automatic Optical Inspection for Steel Golf Club, *2015 12th International Conference on Fuzzy Systems and Knowledge Discovery (FSKD)*. DOI: 10.1109/FSKD.2015.7382317

[5] Wu, F. B., Zhang, X. M., (2014) An inspection and classification method for chip solder joints using color grads and Boolean rules, *Robotics and Computer-Integrated Manufacturing*, **Volume** 30(5), pp. 517–526. DOI: 10.1016/j.rcim.2014.03.003

[6] Wu, H., Zhang, X. M., Kuang, Y. C., Ouyang, G. F., Xie, H. W., (2013) Solder joint inspection based on neural network combined with genetic algorithm, *Optik*, **Volume** 124(20), pp. 4110–4116. DOI: 10.1016/j.ijleo.2012.12.030

[7] Alexandre, R. M., Marcelo, R. S., (2015) Inspecting surface mounted devices using k nearest neighbor and Multilayer Perceptron, *2015 IEEE 24th International Symposium on Industrial Electronics (ISIE)*. DOI: 10.1109/ISIE.2015.7281599

[8] Cai, N., Lin, J. F., Ye, Q., Wang, H., Weng, S. W., Ling, B. W. K. L., (2016) A New IC Solder Joint Inspection Method for an Automatic Optical Inspection System Based on an Improved Visual Background Extraction Algorithm, *IEEE Transactions on components, packaging and manufacturing technology*, **Volume** 6(1). DOI: 10.1109/TCPMT.2015.2501284

[9] Tang, Y. C., Li, L. J., Wang, C. L., Huang, K. Y., (2019) Real-time detection of surface deformation and strain in recycled aggregate concrete-filled steel tubular columns via four-ocular vision, *Robotics Comput.-Integrated Manuf.*, **Volume** 59, pp. 36–46. DOI: 10.1016/j.rcim.2019.03.001

[10] Gong, M., Zhang, Z. J., Zeng, D., Peng, T., (2019) Three-dimensional measurement method of four-view stereo vision based on Gaussian process regression, *Sensors*, **Volume** 19(20), pp. 4486. DOI: 10.3390/s19204486

[11] Tang, Y. C., Li, L. J., Feng, W. X., Chen M. Y., (2018) Binocular vision measurement and its application in full-field convex deformation of concrete-filled steel tubular columns, *Measurement*, **Volume** 130, pp. 372–383. DOI: 10.1016/j.measurement.2018.08.026

[12] Huang, H., Liu, J. H., Liu, S. L., Jin, P., Wu, T. Y., Zhang, T., (2020) Error analysis of a stereo-vision-based tube measurement system, *Measurement*, **Volume** 157. DOI: 10.1016/j.measurement.2020.107659

[13] Hsu, H. W., Lo, Y. L., Lee, M. H., (2019) Vision-based inspection system for cladding height measurement in Direct Energy Deposition (DED), *Additive Manufacturing*, **Volume** 27(6), pp. 372–378. DOI: 10.1016/j.addma.2019.03.017

[14] Eduardo, S. F. S., William, B. X., Ricardo N. R., Silvia S. C. B., (2017) Vision Based Measurement applied to Industrial Instrumentation, *IFAC Papers On Line*, **Volume** 50(1), pp. 788–793. DOI: 10.1016/j.ifacol.2017.08.509

[15] Pagano, S., Russo, R., Savino, S., (2020) A vision guided robotic system for flexible gluing process in the footwear industry, *Robotics and Computer Integrated Manufacturing*, **Volume** 65. DOI: 10.1016/j.rcim.2020.101965

[16] Karunamoorthy, B., Ramprabu, J., (2018) A Novel Method Of real Time Cloth Size Measurement Algorithm Based On Fpga Platform, *International Journal of Innovative Technology and Exploring Engineering (IJITEE)*, **Volume** 8(2S). ISSN: 2278-3075

[17] Li, S., Gerardo, A. C., Simon, R., Jan, P. S., (2018) Autonomous Clothes Manipulation Using a Hierarchical Vision Architecture, *IEEE Access* **Volume** 6, pp. 76646–76662. DOI: 10.1109/ACCESS.2018.2883072

[18] Bradski, G. R., Kaehler, A., (2008) Learning OpenCV, O'Reilly Media, Inc. ISBN: 9780596516130